Journal of Materials Processing Technology 223 (2015) 328–336

Contents lists available at ScienceDirect

Journal of Materials Processing Technology

journal homepage: www.elsevier.com/locate/jmatprotec

Stereo vision based measuring system for online welding path inspection

Drago Bračun*, Alojzij Sluga

University of Ljubljana, Faculty of Mechanical Engineering, Aškerčeva 6, SI-1000 Ljubljana, Slovenia

ARTICLE INFO

Article history:
Received 25 January 2015
Received in revised form 21 April 2015
Accepted 22 April 2015
Available online 30 April 2015

Keywords:
Weld deposit
Arc welding
On-line inspection
Quality evaluation
Welding path
Stereo vision
Measurement

ABSTRACT

A welding path measuring system (WPMS) is developed in order to achieve better understanding of the welding execution of the critical welds or weld deposits in multi-pass and repair welding. The developed WPMS system measures the arc position in 3D space based on the stereo vision principle. The time sequence of arc positions shows a 3D welding path in time, which bears information on how the weld or deposit was welded. Test welding was carried out in order to validate the developed system and to demonstrate how the welding path reveals simulated irregularities in the groove shape and in the electrode motion. The simulated irregularities are visible as anomalies in the welding path. A method for their automatic detection based on the welding path distribution along the weld was proposed.

1. Introduction

For maintaining the quality of the critical welds and weld deposits, significant welding parameters should be monitored on-line and recorded in welding diaries according to the ISO 15609-1 standard. To automate this task, on-line monitoring of electrical welding parameters e.g. voltage and current is widely spread and already embedded in more advanced welding systems. If not, welding systems can be upgraded with voltage and current sensors, microcontroller based data acquisition and signal processing as was demonstrated by Lebar et al. (2012). The correct welding path is also important in multi-pass and reparative welding, where each weld pass should be properly shaped and positioned with respect to the previous deposit to ensure mechanical properties and to prevent the occurrence of slag, cracks and other defects. Ensuring the correct welding path is not problematic in automated welding systems, where the set-up of welding parameters, welding paths and speeds are well-defined and small deviations from the specified path are corrected by seam tracking systems. However, automated welding systems with seam tracking are not always a suitable choice in deposit welding and especially in one-of-a-kind production of large parts. There still exists a lot of manual welding where the welding path is entirely dependent on the welder and thus subject to irregularities. Current market trends urged the need for on-line measuring and inspecting the welding path in non-automated and manual welding. In order to resolve the issue of the unknown welding path, an additional on-line welding path measuring system was needed. The welding path should be measured with contactless method, operating from a safe distance to prevent damage of measuring equipment and not disturbing the welder. When observing the open arc welding from a distance much larger than the arc size, e.g. more than 1 m, the motion of the electrode tip is virtually the same as the arc motion. By measuring the arc motion the welding path can be acquired.

A camera based imaging system is the most advantageous choice for measuring the arc motion. In this paper, a stereo vision based welding path measuring system operating as a supplement to the established on-line monitoring of electrical welding parameters was developed (see Fig. 1). The combination of the welding path measuring system and on-line monitoring of electrical welding parameters has several advantages: a better understanding of weld execution, on-line identification of the welding path non-conformities and consequently, targeted post welding non-destructive testing where irregularities occur.

Ogawa (2011) reviewed the application of high speed imaging to aid the understanding of arc welding phenomena. The imaging systems primarily monitor the phenomena related to the arc, weld pool and electrode tip. The measuring equipment they employ typically consists of a single camera, lens and a narrow pass light filter in front of the lens. The role of the filter is to cut off extreme light

* Corresponding author. Tel.: +386 1 4771 747.
E-mail address: drago.bracun@fs.uni-lj.si (D. Bračun).

http://dx.doi.org/10.1016/j.jmatprotec.2015.04.023
0924-0136/

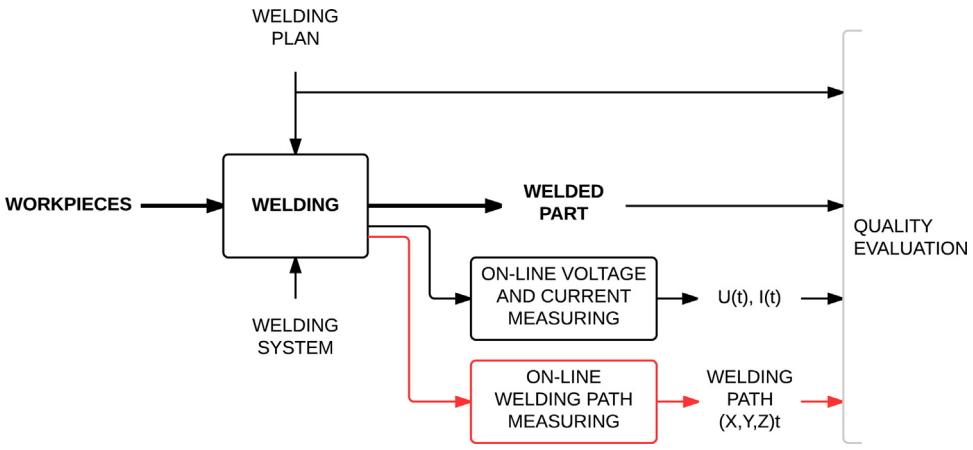

Fig. 1. Welding path measuring system (WPMS) is a supplement to on-line monitoring of electrical welding parameters.

flashes of the arc and to pass only specific wavelengths, typically in the infrared part of the light spectrum emitted by melted metal. Filter based systems are monochromatic systems because they only observe the wavelengths of interest from the emitted spectrum. A color camera is used when an analysis of the entire emitted spectrum is desired. Defect detection with CCD-spectrometer and photodiode-based arc-welding monitoring systems was studied by Mirapeix et al. (2011).

Saeed (2006) summarizes the use of imaging systems in sensing the weld pool state. The ability to observe and measure weld pool surfaces in real-time is the core of the foundation for next generation intelligent welding that can partially imitate skilled welders who observe the weld pool to acquire information on the welding process. Zhang et al. (2013) developed an innovative vision system to project a dot-matrix laser pattern on the weld pool surface in order to measure a three-dimensional weld pool surface in real-time. Wu et al. (2004) developed a vision-based sensing and determination of the weld pool geometrical appearance during the gas-metal arc welding process in order to correlate the surface geometrical appearance of weld pool to the weld penetration and to calculate the prerequisites for process control. Ma et al. (2010) developed a measuring system based on binocular vision sensor to detect both the weld pool geometry and root gap simultaneously for robot welding process.

Additive manufacturing based on gas metal arc welding is an advanced technique for depositing fully dense components with low cost. Techniques to achieve accurate control and automation of the process, however, have not yet been perfectly developed. The online measurement of the deposited bead geometry is a key problem for reliable control. Xiong and Zhang (2013) developed a passive vision-sensing system, comprising two cameras and composite filtering techniques, in order to achieve real-time detection of the bead height and width through deposition of thin walls.

Sun et al. (2005) developed a real-time imaging and detecting system to detect weld defects in steel tube. In the extracted weld seam, based on spatial characteristics near defects—variance and contrast, defects such as slag, blowholes and incomplete penetration are automatically detected using the method of fuzzy pattern recognition. Li et al. (2008) developed visual measurement and inspection of weld bead and defect detection in multilayer welding based on laser structured light vision. The imaging applications play an important role in automated welding systems for seam tracking.

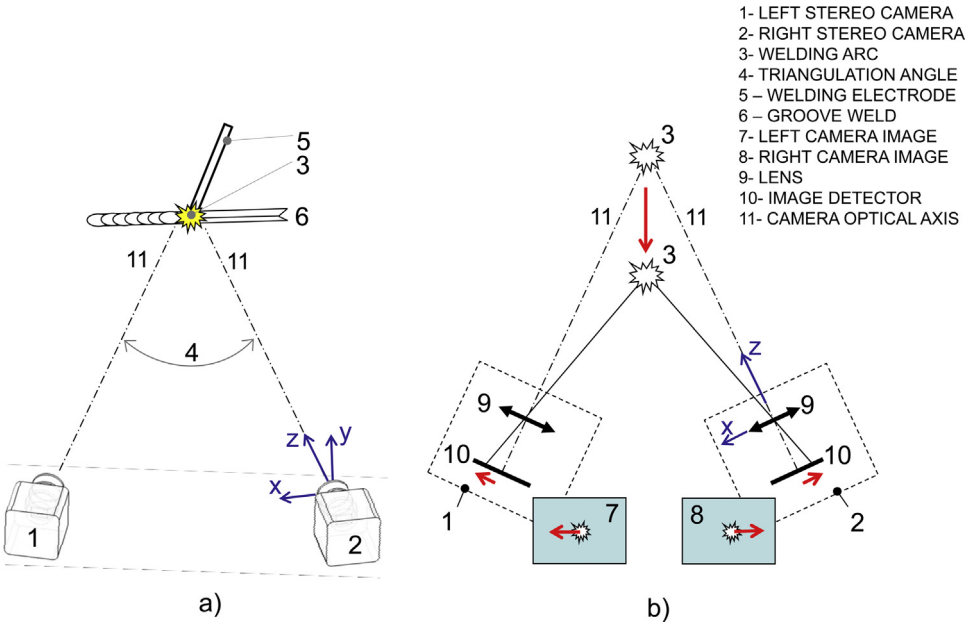

Fig. 2. Measurement setup (a) and operation principle (b).

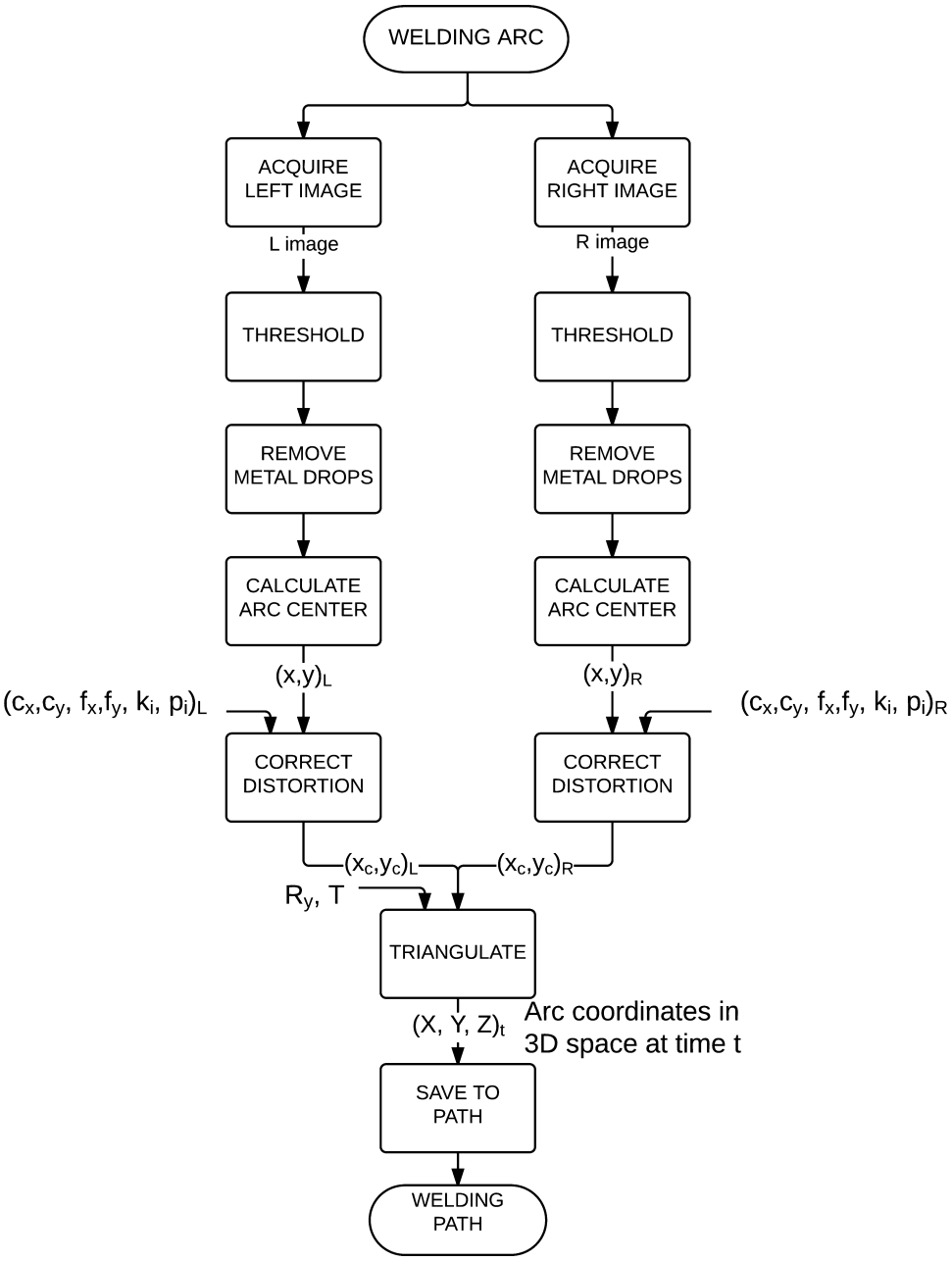

Fig. 3. Calculation of the welding path in 3D space.

2. Welding path measuring system (WPMS)

Important functional requirements when designing WPMS system are: (1) not intrusive for the welder during the welding, (2) robust design appropriate for operation in workshops and (3) parallel and synchronous operation with the system for monitoring electrical welding parameters. The welding path was defined as the time sequence of the arc positions in 3D space. Arc positions in 3D space were measured with a system of two cameras that simultaneously acquired images of the arc (see Fig. 2). The cameras were separated for a particular distance and rotated for an angle with respect to each other to ensure triangulation geometry. The operation principle is demonstrated in Fig. 2b. If the arc is located exactly in the cross section of the cameras' optical axes, the arc image will be positioned exactly in the center of each image. If the arc moves toward the cameras (observe red arrows), its images will go away from the image center and vice versa. The arc location in x–y plane was calculated from the x and y positions of the arc in one of the images, while the z distance was calculated from the disparity of the arc x position in images (see Fig. 4). The mechanical construction provides a parallel alignment of the camera y axes in order to search disparity of the arc centers Δx only along the horizontal x axis. Measurement methods used in 3D stereo vision with CCD cameras and calibration accuracy were evaluated by Aguilar et al. (1996).

It is important to arrange the cameras at a suitable angle with respect to the weld to prevent occlusion of the view on the weld by the welder or work piece geometry, and away from the arc to avoid mechanical damage caused by sparks and excessive heat. For that purpose, telescope lenses were used for close observation of the weld from a considerable distance. Neutral density light filters were also mounted in front of the lenses to block extreme light flashes of the arc. Light sensitivity of the camera detection system, i.e. a camera shutter, gain, iris and neutral density filter, was adjusted to

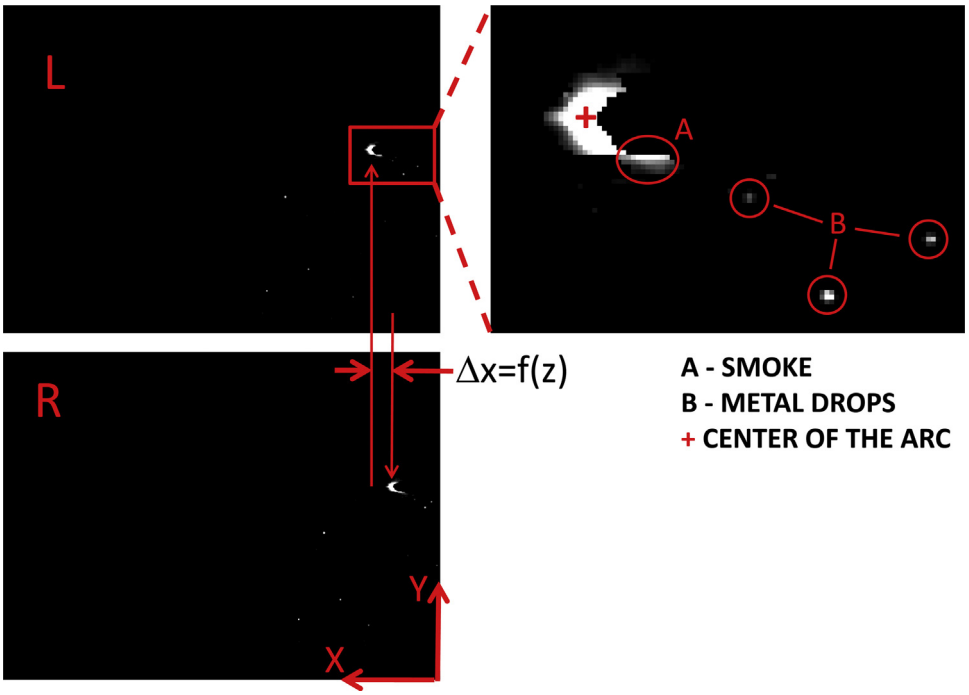

Fig. 4. Typical stereo images of the arc. Left image (L) and right image (R).

observe only the brightest part of the arc between the electrode tip and the melted pool.

The acquired images were processed with algorithm as shown in Fig. 3. To remove the background illumination image threshold was first applied. Second, metal drops that are visible as small bright spots (marked with letter B in Fig. 4) were removed by calculating the area of the spots and by erasing all spots except the largest one which corresponds to the arc. Finally, the arc center was calculated by applying the center of gravity algorithm in two dimensions.

The position of the arc center in a particular image (x, y) exhibits position errors originating from lens distortion. In order to correct them, the arc center was normalized initially e.g. expressed in angles with respect to the optical axis:

$$(x_n, y_n) = \left(\frac{x - c_x}{f_x}, \frac{y - c_y}{f_y} \right). \quad (1)$$

In Eq. (1) subscript n denotes normalized coordinates, (c_x, c_y) is a point where optical axis intersects the image and (f_x, f_y) is the lens focal length in x and y axis, respectively. Distortion errors were corrected by applying an iterative algorithm:

START: $r = \sqrt{x_n^2 + y_n^2}$

$$k_r = 1 + k_1 \cdot r^2 + k_2 \cdot r^4$$

$$\Delta x_t = 2 \cdot p_1 \cdot x_n \cdot y_n + p_2 \cdot \left(r^2 + 2 \cdot x_n \right)$$

$$\Delta y_t = p_1 \cdot \left(r^2 + 2 \cdot y_n \right) + 2 \cdot p_2 \cdot x_n \cdot y_n$$

$$(x_c, y_c) = \frac{1}{k_r} (x_n - \Delta x_t, y_n - \Delta y_t)$$

IF $(x_c - x_n < tol)$ and $(y_c - y_n < tol)$
THEN x_c, y_c are distortion free
END;
ELSE $x_n = x_c$; $y_n = y_c$;
GOTO START.

In this algorithm, (x_c, y_c) are distortion free arc coordinates, k_r is a radial distortion with parameters k_1 and k_2, Δx_t and Δy_t are the tangential distortion in x and y axes with parameters p_1 and p_2. The tolerance $tol = 10^{-6}$ is typically achieved in a few iterations. Arc coordinates in 3D space were calculated from the corrected arc coordinates in the left $(x_c,y_c)_L$ and right $(x_c,y_c)_R$ image, and by knowing the relative positions of the cameras. Because the mechanical construction provides a parallel alignment of the camera y axis, triangulation can be carried out only in x–z plane. Point p within view field of both cameras can be expressed in the left or in the right camera coordinate system. The relation between the two coordinate systems is:

$$P_L = R_y \cdot P_R + T. \quad (2)$$

In this equation $P_L = (X_L,Z_L)^T$ is a coordinate of the point expressed in the left camera coordinate system and $P_R = (X_R,Z_R)^T$ is the same point expressed in the right camera coordinate system. Both P_L and P_R are Cartesian coordinates in millimeters. The rotation matrix $\boldsymbol{R}_y = [\cos(\varphi),-\sin(\varphi);\sin(\varphi),\cos(\varphi)]$ gives a relative rotation of the cameras around y axis for the angle φ, and $T = (Tx,Tz)^T$ gives the displacement of the cameras in x–z plane. Point coordinates in 3D space can be expressed with corresponding normalized coordinates multiplied by a Z distance as $P = Z \cdot (x_c,y_c)$. If this is applied in Eq. (2), triangulation equations are derived

$$x_{cL} \cdot Z_L = \cos(\varphi) \cdot x_{cR} \cdot Z_R - \sin(\varphi) \cdot Z_R + T_x, \quad (3)$$

$$Z_L = \sin(\varphi) \cdot x_{cR} \cdot Z_R + \cos(\varphi) \cdot Z_R + T_z. \quad (4)$$

The unknown variables in Eqs. (3) and (4) are Z_L and Z_R. Solving the equations for Z_R results in:

$$Z_R = \frac{T_x - x_{cL} \cdot T_z}{\sin(\varphi) \cdot (x_{cL} \cdot x_{cR} + 1) + \cos(\varphi) \cdot (x_{cL} - x_{cR})}. \quad (5)$$

The arc location in 3D space has thus coordinates $Z_R \cdot (x_c,y_c,1)_R$ if expressed in the right camera coordinate system, or $Z_L \cdot (x_c,y_c,1)_L$ if expressed in the left camera coordinate system.

3. Calibration

For each camera 8 internal parameters have to be determined: the intersection of the optical axis with the image (c_x, c_y), focal

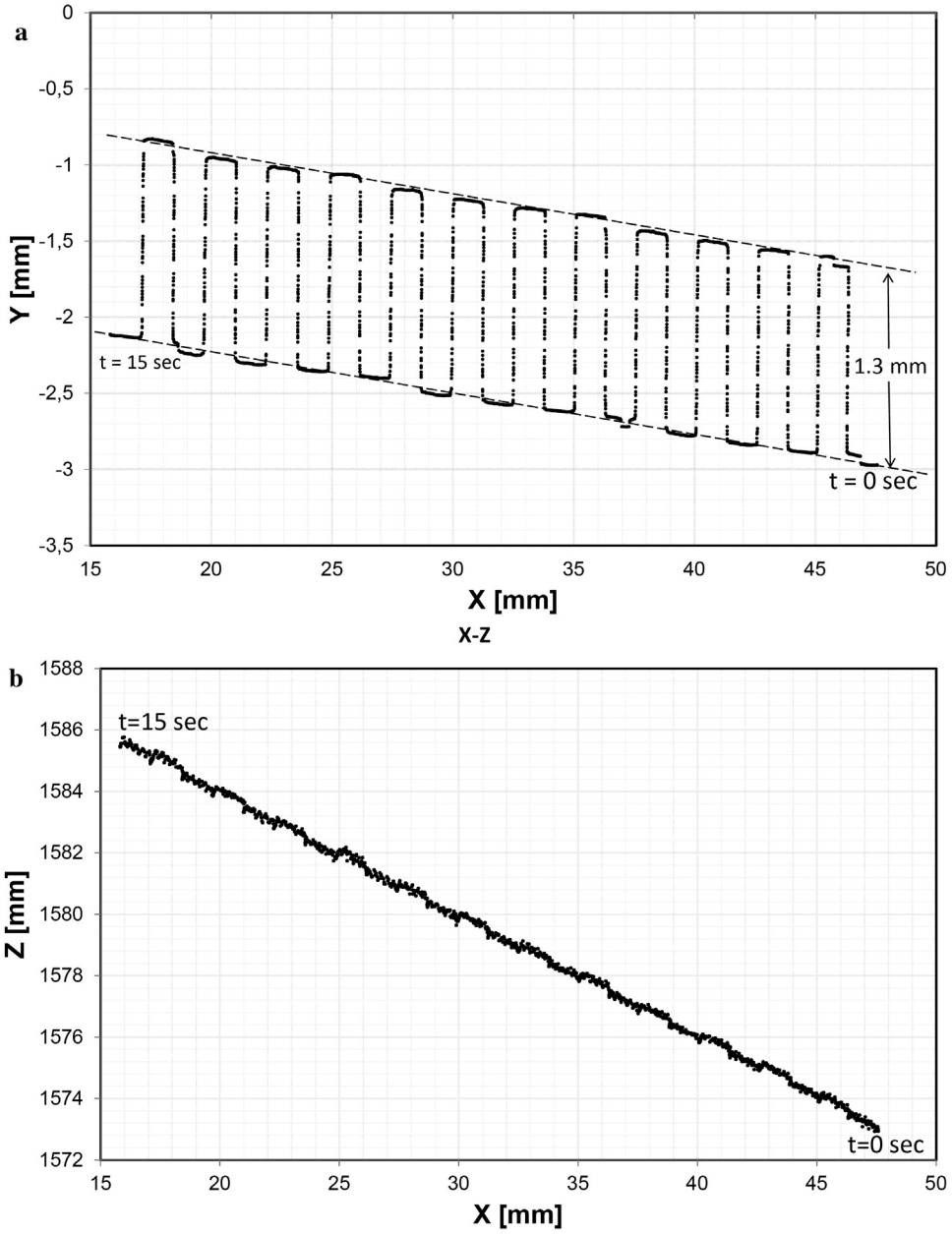

Fig. 5. Test measurement of a reference path.

length (f_x, f_y), lens radial distortion (k_1, k_2) and lens tangential distortion (p_1, p_2). For both cameras that is 16 parameters. By assuring a parallel alignment of the camera y axis, three additional external parameters should be determined: the angle φ of the camera rotation and displacement of the camera centers T_x and T_z. Camera calibration (Bouguet, 2013) was used in order to calibrate the system. Each camera was initially separately calibrated in order to determine internal parameters. External parameters were determined with respect to the reference checkerboard.

4. Measuring properties

Measurement speed is defined as the number of positions measured per second. It should be high enough to capture the waving motion of the electrode tip. We estimate that the welder does up to five waves per second. To capture this motion, the sampling frequency should be at least 100 samples per second. In camera based measurement systems, the sampling frequency is defined by a number of images that a camera acquires per second (frame-rate). To get its maximum, fast cameras with an embedded programmable logic that enables a simultaneous acquisition and pre-processing of 200 images per second are applied. The time stamp is assigned to each pair of stereo images, which enables a comparison of the arc position to the simultaneously acquired electrical parameters. The measuring field is defined with a cross section of the left and right camera view fields (0.3 m width × 0.3 m height at 1.5 m distance from the cameras in our case). To estimate measurement uncertainty of the WPMS system, the discrepancies between the reference path motion (such as input in the measuring system) and measured path motion (such as output of the system) were analyzed. The reference path motion was generated by a three-axis CNC milling machine with positioning accuracy of 0.01 mm. The arc was simulated with a bright LED diode attached to the cutting tool. The 1.3 mm square zig-zag input motion is

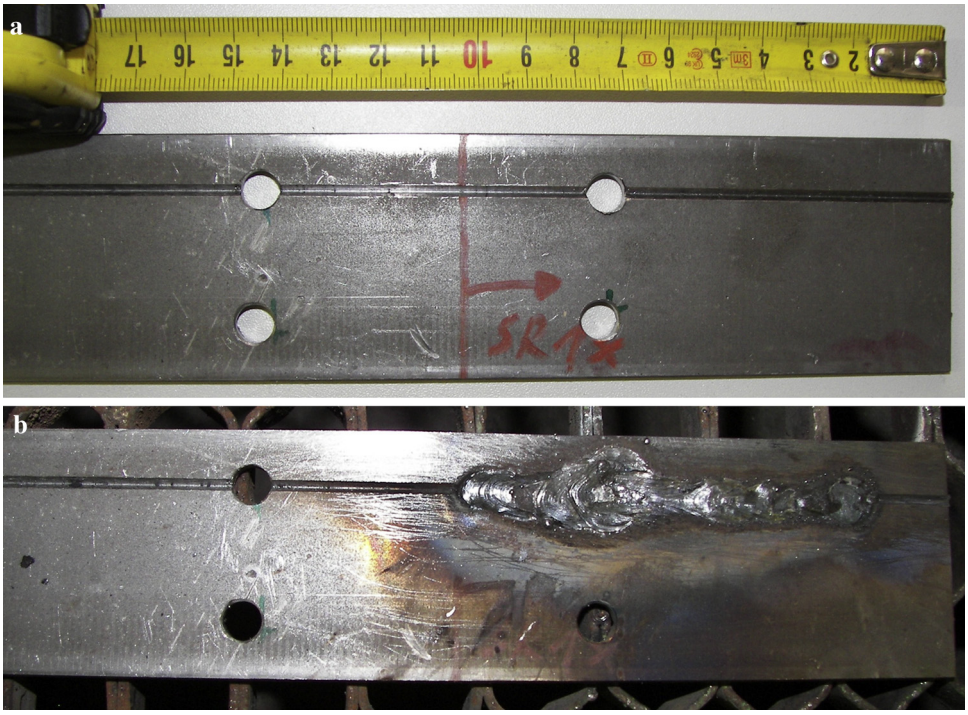

Fig. 6. Test part with simulated irregularities (holes) in the groove before welding (a) and after the welding (b).

demonstrated. The measured path is shown in Fig. 5. The square shape is clearly visible in a measurement system x–y plane, while the diode to measurement system distance and path straightness is visible in x–z plane.

The standard deviation of 0.27 mm of the discrepancies between the measured path and reference motion is found and used as an estimate of type A measuring uncertainty. Type B uncertainty originating from the irregularly changing shape of the arc and from the illuminated smoke is also found (see Fig. 4). The illuminated smoke is visible in the close proximity of the arc. Further away it is dispersed and not bright enough to be observable with the detection system whose sensitivity is adjusted to the brightest part of the arc. By applying the center of gravity algorithm on the image with visible smoke, the arc center can be shifted up to a few pixels. Consequently the calculated arc coordinates in 3D space are also displaced. For that reason, the amount of noise in the measured path is larger in actual welding than in the case of LED diode motion. From noise observations in test measurements type B measuring uncertainty i.e. evaluation of uncertainty by non-statistical methods is estimated to 1 mm. The analysis of measuring uncertainty shows that the developed system is appropriate for measuring the electrode tip motion in cases when this is larger than 1 mm.

5. Validation experiments

In order to validate the developed WPMS, a measurement of the welding path with simulated irregularities in the groove shape and in the electrode motion was carried out. Fig. 6 shows the sample part before (a) and after the welding (b) with a coated steel electrode. Before the welding the "V" shaped groove was interrupted with simulated irregularities, i.e. two holes whose diameter (ϕ8 mm) is much larger than the groove width (3 mm). The welder had to fill them by welding around the holes. Defects like cracks, slag and small bubbles are expected in this location. In order to reduce the influence parameters on welding path measurement e.g. out-of-plane displacements resulting from thermal deformations, the initial test samples were prepared from a single thick plate and the grooves were milled out of it. The samples were also clamped to the support in order to prevent incidental shifts by the welder. The measured path is shown in orthographic projections in two perpendicular planes in Fig. 7. The first $x(z)$ graph has the same view point as the image of the weld in Fig. 6b. It is clearly seen how the welder welded around the hole to fill it. The second graph is $y(z)$ and shows a vertical motion. The third $\delta(z)$ graph represents the relative distance $\delta(i)$ from the beginning of the weld up to the particular position $z(i)$:

$$\delta(i) = \frac{d(i)}{L} \cdot 100 = \frac{\sum_{j=0}^{i} \sqrt{\left(x_{j+1}-x_j\right)^2 + \left(y_{j+1}-y_j\right)^2 + \left(z_{j+1}-z_j\right)^2}}{\sum_{j=0}^{n} \sqrt{\left(x_{j+1}-x_j\right)^2 + \left(y_{j+1}-y_j\right)^2 + \left(z_{j+1}-z_j\right)^2}} \cdot 100\,[\%]\,. \tag{6}$$

The relative distance $\delta(i)$ is expressed in percentage of total welding path length L, where n is the number of all points in the path and indices i and j run from 0 to n and from 0 to the particular position i, respectively. In Fig. 7 the weld is oriented along the measurement system z axis. If the welder intuitively does some movements to correct something, for example to fill the hole, the z coordinate at the hole will not change. However, the total length of the path will increase because of this additional motion around the hole. In $\delta(z)$ graph this is visible as a vertical segment of the curve in range from 1480 to 1490 mm. Vertical segments in $\delta(z)$ curve are an indicator that something has happened there. The shape and slope of $\delta(z)$ curve bear the information about the welding speed and welding direction. If the shape is linear, the welding speed is constant. The slope informs us about the welding direction and the amount of weaving with respect to the main welding motion. In case of a narrow groove, the total length will not increase as fast as in the case of the wide groove, where the welder did a lot of waving to fill the groove.

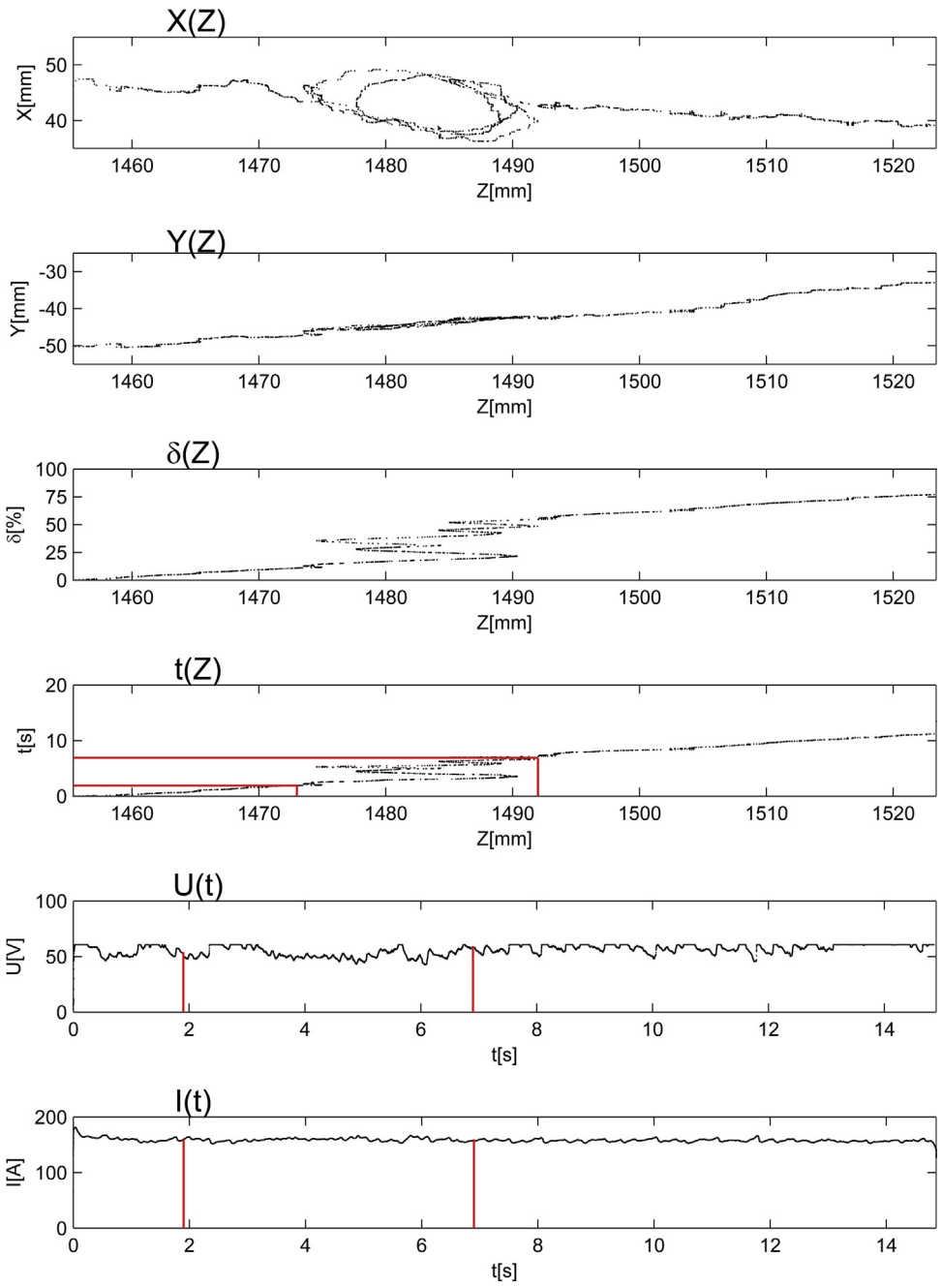

Fig. 7. The measured welding path and corresponding electrical welding signals

If electrical welding current and voltage are synchronously acquired with the welding path, they can be correlated based on the same time basis as is demonstrated in the fourth graph $t(z)$. That shows a welding path in relation to the time of welding. The horizontal axis z is equal as in the first three graphs, while the vertical axis, i.e. time, corresponds to the last two graphs showing the welding voltage $U(t)$ and current $I(t)$ in relation to time. The time of welding is expressed in seconds since the beginning of the weld. In general the shape of $t(z)$ graph is similar to $\delta(z)$ graph. Many modern welding power supplies enable automated acquisition of electrical parameters; however, synchronization with external devices is typically not possible. For that reason a custom developed monitoring system was applied and added to the welding power supply. In $\delta(z)$ graph a vertical part of curve is in range from 1480 to 1490 mm. In $t(z)$ graph this corresponds to the welding time between 2 and 7 s. A quick inspection of $U(t)$ and $I(t)$ shapes in this time interval does not show any significant pattern that would lead to identifying the hole. The filled hole may not even be visible in the external shape of the weld. However, it can be the source of several defects like slag, cracks and inhomogeneous material. Knowing the welding path has a great potential for a targeted post welding non-destructive inspection.

6. Automatic detection of welding path irregularities

Fig. 8 shows an application where a large kitchen pot was assembled from stainless steel sheets of 1 mm in thickness which are welded together at the right angle. Welding was carried out by manual gas tungsten arc welding (GTAW) without filler material. Here the selection of welding parameters and the welder's experience play an important role in creating a successful weld in terms of different requirements e.g. mechanical, water resistant,

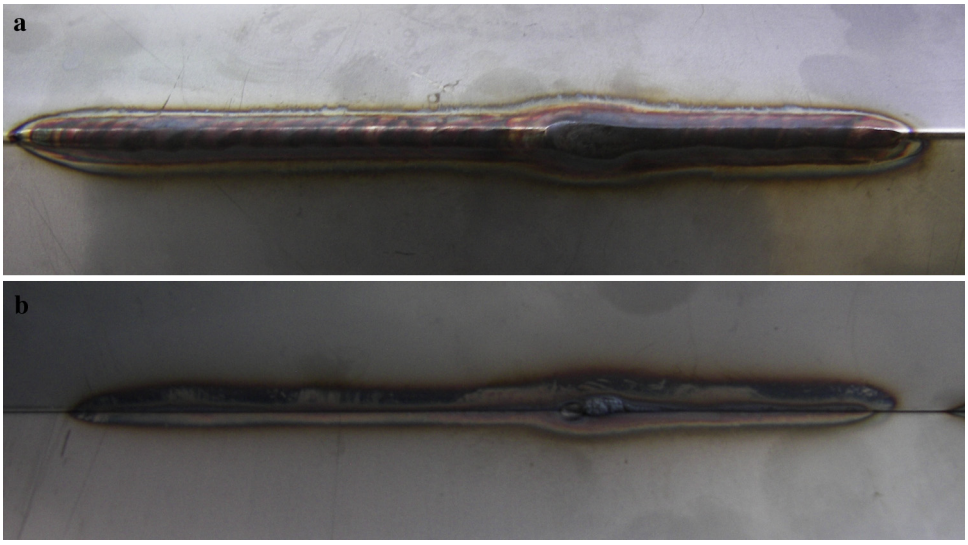

Fig. 8. Stainless steel sheets after the welding. Top view (a) and root view (b) on the weld.

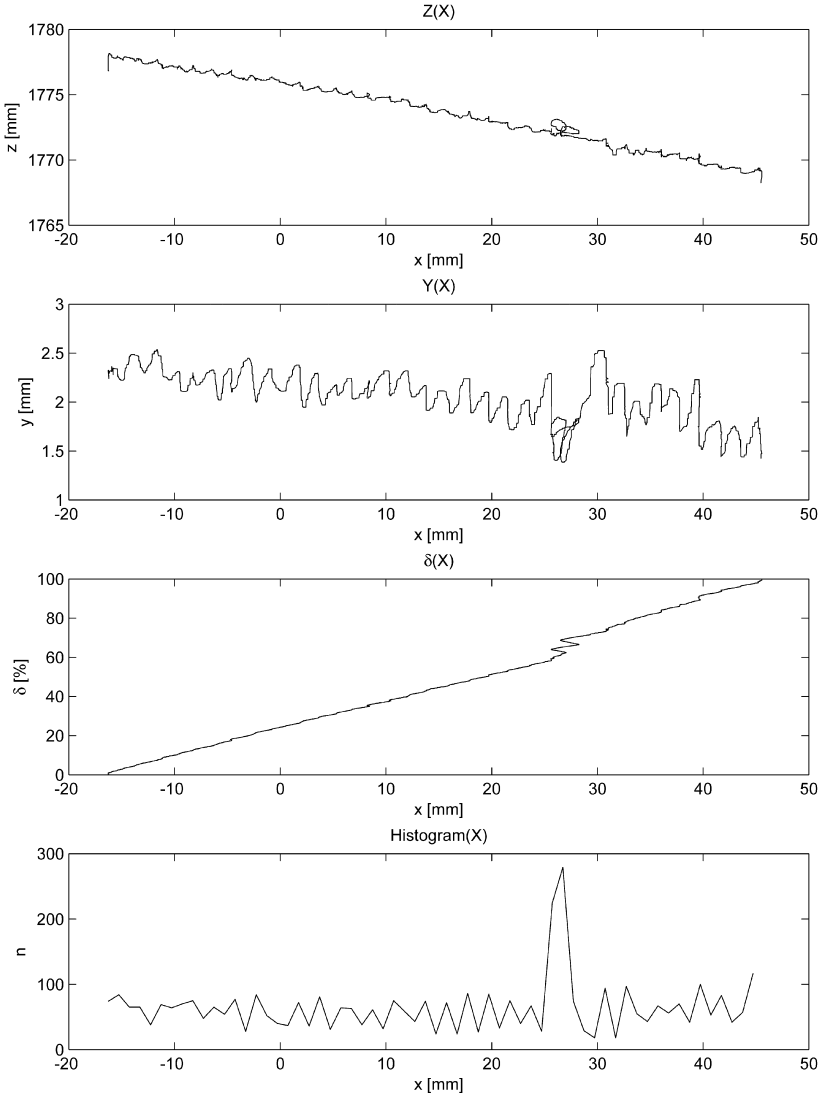

Fig. 9. Graphs of the welding path.

hygienic and aesthetic. The welder was instructed to intentionally create an irregularity by staying a little longer at a particular position. The energy input was greater, the material was more melted, which resulted in the final shape of the weld. The welding path is shown in Fig. 9.

The $z(x)$ graph of the welding path shows the top view of the weld, while the $y(x)$ graph shows the vertical motion. It is clearly visible that the welder performed some additional motion in the range between 25 and 30 mm. The relative distance $\delta(x)$ also shows the vertical segment in this range. An automatic identification of such vertical segment was carried out by calculating the distribution of the welding path along the weld. For this purpose, the weld was initially oriented approximately along the measurement system x axis. The x coordinate is split into bins, and the number of arc positions with each bin is calculated to obtain the welding path distribution along the weld; see fourth graph. A significant peak occurred in the observed range. By applying control limits e.g. 200, this peak was automatically recognized. The calculation of the histogram is simple when the weld is aligned with one of the coordinate axes. If this is not the case, the coordinate system should initially be aligned with the weld.

7. Conclusions

- This paper presents the development of a stereo vision measuring system (WPMS) for an on-line welding path inspection in order to acquire information about the welding path, welding direction, welding speed and the amount of the electrode waving motion in an automated way.
- Irregularities in the groove shape or in the electrode motion are visible as anomalies in the 3D welding path.
- The anomalies can be automatically detected by analyzing the welding path distribution along the weld.
- The welding path can be compared to the simultaneously acquired electrical welding current and voltage signals based on the same time basis.
- Knowing the welding path has a great potential for a targeted post welding non-destructive inspection, which is proposed for future research.
- In addition, the developed WPMS system could be used in other applications, i.e. more comprehensive and automated on-line data recording to the welding diaries, training of welders, etc.

Acknowledgements

This work was supported by the Ministry of Higher Education, Science and Technology of the Republic of Slovenia, Grant no. 630-36-2014-1.

Appendix A. Supplementary data

Supplementary data associated with this article can be found, in the online version, at http://dx.doi.org/10.1016/j.jmatprotec.2015.04.023

References

Aguilar, J.J., Torres, F., Lope, M.A., 1996. Stereo vision for 3D measurement: accuracy analysis, calibration and industrial applications. Measurement 18, 193–200, http://dx.doi.org/10.1016/S0263-2241(96)00065-6

Bouguet, J.-Y., 2013. Camera calibration toolbox for Matlab. Comput. Softw., http://www.vision.caltech.edu/bouguetj/calib_doc/index.html.

Lebar, A., Selak, L., Vrabič, R., Butala, P., 2012. Online monitoring, analysis, and remote recording of welding parameters to the welding diary. J. Mech. Eng. 58, 444–452, http://dx.doi.org/10.5545/sv-jme.2012.341

Li, Y., Qing, L.W., You, F.L., Xu, D., Tan, M., 2008. On-line visual measurement and inspection of weld bead using structured light. In: Conference Record—IEEE Instrumentation and Measurement Technology Conference, pp. 2038–2043.

Ma, H., Wei, S., Lin, T., Chen, S., Li, L., 2010. Binocular vision system for both weld pool and root gap in robot welding process. Sens. Rev. 30, 116–123, http://dx.doi.org/10.1108/02602281011022706

Mirapeix, J., Ruiz-Lombera, R., Valdiande, J.J., Rodriguez-Cobo, L., Anabitarte, F., Cobo, A., 2011. Defect detection with CCD-spectrometer and photodiode-based arc-welding monitoring systems. J. Mater. Process. Technol. 211, 2132–2139.

Ogawa, Y., 2011. High speed imaging technique Part 1—High speed imaging of arc welding phenomena. Sci. Technol. Weld. Joining 16, 33–43, http://dx.doi.org/10.1179/136217110X12785889549903

Saeed, G., 2006. Vision-based sensing of the welding process: a survey. Int. J. Model. Ident. Control 1, 84–93, http://dx.doi.org/10.1504/IJMIC.2006.010103

Sun, Y., Bai, P., Sun, H., Zhou, P., 2005. Real-time automatic detection of weld defects in steel pipe. NDT E Int. 38, 522–528, http://dx.doi.org/10.1016/j.ndteint.2005.01.011

Wu, C.S., Gao, J.Q., Zhang, M., 2004. Sensing weld pool geometrical appearance in gas–metal arc welding. Proc. Inst. Mech. Eng. B J. Eng. Manuf. 218, 813–818, http://dx.doi.org/10.1177/095440540421800714

Xiong, J., Zhang, G., 2013. Online measurement of bead geometry in GMAW-based additive manufacturing using passive vision. Meas. Sci. Technol. 24, 115103.

Zhang, W., Wang, X., Zhang, Y., 2013. Analytical real-time measurement of a three-dimensional weld pool surface. Meas. Sci. Technol. 24, 115011, http://dx.doi.org/10.1088/0957-0233/24/11/115011.